Applied Catalysis A: General 474 (2014) 26–33

Contents lists available at ScienceDirect

Applied Catalysis A: General

journal homepage: www.elsevier.com/locate/apcata

Synthesis of a catalyst of Mn–Fe–O by mechano-chemical reaction

María M. Barroso Quiroga, Bibiana P. Barbero, Luis E. Cadus*

Instituto de Investigaciones en Tecnología Química (INTEQUI), UNSL–CONICET, Chacabuco 917, D5700BWS San Luis, Argentina

ARTICLE INFO

Article history:
Received 19 December 2012
Received in revised form 2 September 2013
Accepted 4 September 2013
Available online 16 September 2013

Keywords:
Ball milling
Nanocrystalline materials
Manganese iron oxides, VOC catalytic combustion

ABSTRACT

In this work, the Fe–Mn–O system was mechanically processed in a high-energy ball-milling. The as milled powders were characterized by X-ray diffraction (XRD), temperature programmed reduction (TPR), X-ray photoelectron spectroscopy (XPS) and specific surface area measurement. Catalytic total oxidation of *n*-hexane was studied to find out the suitability of the material for VOC decomposition reaction. The route of the solid state transformation of Mn–Fe–O system has been established as a function of the cumulated energy from mechanical milling. Complex multicomponent catalysts, which may be difficult to prepare by conventional high temperature treatment, have been successfully prepared by milling.

1. Introduction

The objective of research on nanoscience may be summarized in three aspects: synthesis, understanding and exploration of new nanomaterials, and the related phenomena. It is widely accepted that nanosized magnetic materials exhibit different properties compared with bulk materials [1–4]. When the size of a particle becomes smaller and smaller to the finite size, the surface effects play an important role in various properties of materials [5–7]. This brings a renewed interest in the study of different properties of pure and mixed oxide systems in nanocrystalline regime. In catalysis, the characteristic of the surface is the most important factor. High-energy ball milling is the earliest nanoparticle preparation method that has been applied to industrial production among those nanoparticle synthesis technologies [8]. A wide variety of techniques are being used to synthesize nanostructured materials including gas condensation, rapid solidification, electrodeposition, sputtering, crystallization of amorphous phases and chemical processing [9]. The high-energy ball milling has become a popular method to make nanocrystalline materials because of its simplicity and the relatively inexpensive equipment needed, as well as the applicability to essentially all classes of materials. The major advantage often quoted is the possibility for easily scaling up to tonnage quantities of material in a number of applications. In fact, contamination problems are frequently given as a reason to dismiss the method at least in relation to some materials [8]. In the past, the effectiveness of a milling process has been assessed in terms of changes in the particle shape, size and size distribution.

The Mn-Fe-O system has been proposed as an excellent catalyst for catalytic combustion [10]. The Mn_2O_3 is a stable phase. MnO_x is capable of mobilizing electrons and, thus, of generating the mobile-electron environment required by redox catalysts. Mn_2O_3 can absorb oxygen and act, in an oxidizing atmosphere, as p-type semiconductors. This is due to the possibility of Mn cation to reach the tetravalent state. An n-type semiconductor, like Fe_2O_3, cannot be further oxidized. Duran et al. [10] have prepared Mn_2O_3–Fe_2O_3 mixtures by the citrate method. They showed that these materials are active catalysts for the catalytic oxidation of volatile organic compounds at low temperatures. The formation of several arrangements such as solid solution or $Fe_xMn_yO_4$ spinels has been proposed. The physico-chemical properties of ferrites are strongly dependent on the site, nature and amount of the metal incorporated in the structure. There are not many oxide systems studied by high energy ball milling (HEBM). Schaffer and McCormick [11] were the first to report the mechano-chemical reduction of metal oxides by a more reactive metal ($CuO + Ca \rightarrow Cu + CaO$). In a subsequent publication [12], these authors have reported similar mechano-chemical reduction reactions in a number of systems ($Ag_2O + Al$; $ZnO + Ca$; $ZnO + Ti$; $V_2O_5 + Ti$; $Fe_2O_3 + Ca$; $CuO + Me$, where Me = Al, Fe, Mg, Mn, Ni). In ball-milling experiments involving pure α-Fe_2O_3 [13–17] or mixtures of α-Fe_2O_3 and SiO_2 in air [18], reduction of α-Fe_2O_3 to Fe_3O_4 was observed to occur in a closed stainless steel container after prolonged milling. More recently, Medeiros et al. [19] have mechanically processed the $(Fe_2O_3)_x(Mn_2O_3)_{1-x}$ and $Fe_y(Mn_2O_3)_{1-y}$ systems in a high-energy ball-mill. These systems were submitted to mechanical milling and their structural, magnetic and Mossbauer characteristics were investigated. In the oxide–oxide system, a $(Fe,Mn)_2O_3$ solid solution with the bixbyite

* Corresponding author. Tel.: +54 265 7430537/+54 266 4426711; fax: +54 266 4426711.
E-mail address: lcadus@unsl.edu.ar (L.E. Cadus).

0926-860X/$ – see front matter © 2013 Elsevier B.V. All rights reserved.
http://dx.doi.org/10.1016/j.apcata.2013.09.001

structure was formed for any hematite starting concentration. The obtained bixbyite phase had two iron sites and showed a magnetic transition at ~40 K. However, those authors have limited their studies to the use of a vial and balls of hardened steel, under air atmosphere. With milling conditions such as ball-to-powder mass ratio (30:1), rotation velocity (300 rpm) and milling time (24 h), all kept constant throughout the experiments, the accumulated energy was low.

Furthermore, the Mn-Fe system has been extensively studied to obtain the spinel ferrite $MnFe_2O_4$. Ding and his coworkers [20] found that Mn_2O_3 and Fe_2O_3 ball-milled for 66 h under an argon atmosphere resulted in the formation of disordered $MnFe_2O_4$. Nanoparticles of spinel ferrites are of great interest in fundamental science for addressing relationship between physical properties and their crystal structure and chemistry. Ferrites represent a class of materials extensively studied, thanks to their electrical and magnetic properties. These materials are widely used both in electrical and electronic industry for the fabrication of devices and components such as high-density magnetic core of read/write heads for high-speed tape or disk recording. Besides the traditional application, a renewed interest is now emerging in different fields such as biomedical science [21,22] or in sustainable energy research. It has been proved that some ferrites can be successfully used in low-temperature water splitting thermochemical cycles [23–25].

In the majority of the cases, the HEBM synthesis of $MnFe_2O_4$ was carried out under argon atmosphere by mechanically activated solid-state reaction of a stoichiometric mixture of the reagents. Most of the works have used MnO or MnO_2 as starting manganese oxides, vial and balls of stainless steel, and the lowest energy of milling.

Reduction processes induced by mechanical treatment represent an important and significant class of mechano-chemical solid state reactions. Mn-Fe-O system offers a large number of combinations of steps and arrangements of steps, which result catalytically interesting [10]. Kedesdy and Tauber [26] have published the phase diagram showing the formation of manganese ferrite under different conditions. Recently, it has become apparent that in order to characterize more fully a powder, account must be taken of the strain content induced during the milling process. Although in the literature there are scores of research articles describing the effect of grain size on magnetic properties of spinel ferrites synthesized by several chemical routes including ball milling, no details of the solid state reaction during the transformation into the spinel phase are available. A perusal of the literature indicates that these particular aspects, i.e. mechanical milling induced strain and its effect on structural properties of Mn-Fe oxides, have not been investigated in detail or correlated with the accumulated energy, though all other physical properties are decisively dependent on structure, grain morphology and cation distribution in the spinel ferrite system. We feel that this study will provide a new dimension in the area of nano-sized ferrite materials and structure–property correlation.

Herein, we report the effect of the accumulated energy from mechanical grinding on the morphology, structural properties and synthesis route of Mn–Fe–O oxides.

By investigating a new promising field of applications, we will show how the preparation of materials having a high surface area and/or presenting structural defects can lead to a material with interesting catalytic properties. In the field of total catalytic oxidation, a lot of work has been devoted to this subject. This mixing brings the formation of supplementary lattice defects, which are believed to play a major role in the catalytic activity of the sample. Up to now, oxide catalysts were mainly synthesized by solid state reaction and chemical solution method. The former, involving a high-temperature ceramic process, leads to materials exhibiting low surface area and large particle size, whereas the latter is a complicated process with several steps.

Duran et al. [10] prepared a fine catalyst, following the citrate method. It has a Fe:Mn atomic ratio equal to 1:3, and was calcined in air at 500 °C. It has a 60 $m^2\ g^{-1}$ BET surface area, and its XRD diffraction lines are from α-Mn_2O_3 (bixbyite), and α-Fe_2O_3 (hematite). This catalyst is our reference catalyst, and our aim is to prepare it following a mechanochemical method.

The benefit of mechano-chemistry on the catalytic properties of Mn–Fe–O oxides will be demonstrated. In addition, a catalyst with an excellent performance in VOC combustion can be obtained regulating the cumulative energy.

2. Experimental

2.1. Catalyst preparation

The solid-state reaction of a fixed atomic ratio of Mn:Fe = 3:1 was mechanically activated from a mixture of Mn_2O_3 and Fe_2O_3. The starting reagents were commercial Fe_2O_3 powder (Fluka) and Mn_2O_3 obtained by thermal decomposition of manganese carbonate (Fluka) calcined in air at 600 °C for 1 h. The ball milling processes were carried out using a planetary ball milling (Fritsch Pulverissette 6) equipped with cylindrical tungsten carbide vials (80 cm^3) together with 15 mm diameter agate and WC balls. The ball mass–powder mass ratio was fixed at two levels: 10:1 and 35:1. The rotation speed was fixed at two levels, 300 and 500 rpm. As result of the combination of the ball mass–powder mass ratios and the rotation speeds, three series of catalysts were prepared:

Series A: low energy (300 rpm and BPR of 10:1), agate balls.
Series B: medium energy (500 rpm and BPR of 10:1), agate balls.
Series C: high energy (500 rpm and BPR of 35:1), WC balls.

Milling time: 1 min (A0, B0, C0), 5 h (A5, B5, C5), 10 h (A10, B10, C10) and 20 h (A20, B20, C20).

After mechanical milling the catalysts were calcined at 350 °C during 3 h.

2.2. Characterization

2.2.1. BET specific surface area

The specific surface area of catalysts was calculated by the BET method from the nitrogen adsorption isotherms at 77 K after outgassing the samples at 250 °C by using a Micromeritics Gemini V apparatus.

2.2.2. X-ray diffraction (XRD)

XRD patterns were obtained by using a Rigaku diffractometer operated at 30 kV and 25 mA by V-filtered Cr *K*α radiation (λ = 0.2291 nm), 3° min^{-1} scan velocity. The crystalline phases were identified by reference to powder diffraction data (PDF).

2.2.3. Temperature programmed reduction (TPR)

The TPR was performed in a quartz U-type tubular reactor using a TCD as detector. A 40-mg sample was used. The reducing gas was a mixture of 5 vol% H_2/N_2, at a total flow rate of 30 ml min^{-1}. The temperature was increased at a rate of 15 °C min^{-1} from room temperature to 700 °C; then, it was kept constant at 700 °C until the signal of hydrogen consumption returned to the initial values.

2.2.4. X-ray photoelectron spectroscopy (XPS)

The XPS analyzes were performed in a multi-technique system (SPECS) equipped with an Al-monochromatic X-ray source, and a hemispherical PHOIBOS 150 analyzer operating in the fixed analyzer transmission (FAT) mode. The spectra were obtained using a monochromatic Al *K*α X-ray source ($h\upsilon$ = 1486.6 eV) operated at 150 W and the pass energy for the element scan was 30 eV.

The working pressure in the analyzing chamber was less than 2×10^{-8} mbar. The data treatment was performed with the Casa XPS program (Casa Software Ltd, UK). The peak areas were determined by integration, employing a Shirley-type background. Peaks were considered to be a mixture of Gaussian and Lorentzian functions. For the quantification of the elements, sensitivity factors provided by the manufacturer were used.

2.3. Catalytic test

The catalysts were evaluated in total oxidation of *n*-hexane as representative volatile organic compound (VOC) using a quartz reactor of fixed bed. The catalyst powder was pressed, crushed and sieved to a size of 80–100 mesh (0.18–0.15 mm) for catalytic evaluation and then, a 200-mg sample was diluted with glass of the same size as that of the catalyst and in a volumetric ratio of 1:23. The total flow was 200 ml min^{-1} with 4000 mg C m^{-3} of *n*-hexane. The temperature, measured with a coaxial thermocouple, varied between 80 and 350 °C, increasing in steps of 20 °C. The data reported at each reaction temperature were the average of at least two steady-state measurements. The reagents and products of reaction were analyzed on line by using a GC equipment.

3. Results and discussion

In this work, phase transformation during milling using the mechanical milling parameters as reference has been presented. It is well known that mechano-chemical reactions are promoted by the energy transferred from the milling bodies to the milled powder. In order to favor a comparison between different milling conditions, results are discussed using as parameter the cumulative kinetic energy released in the system. It includes ball-impact energy, ball-impact frequency, milling time and powder weight carried out by Burgio et al. [27], and systematized in a milling map by Rojac et al. [28]. According to these authors, a total of nine parameters are required to describe the process which can be further divided in terms of the milling balls, milling vial, milling operation and mill characteristics. As it is known, the conventional high energy ball milling needs calcinations at high temperature in order to assure high crystallinity and stability; but in the case that a prepared solid is used as catalyst, it is necessary to maintain the specific surface area and the calcination at high temperature is not convenient because it favors the sintering process. For this reason, the cumulated energy used was higher than that of previous works published in the literature. Table 1 shows the cumulative energy for each sample, calculated from the following equations [28].

$$\Delta E_b = \left[\frac{1}{2}\left(\rho_b \frac{\pi d_b^3}{6}\right) W_p^2 \left(\frac{W_v}{W_p}\right)^2 \left(\frac{D_v - d_b}{2}\right)^2 \left(1 - 2\frac{W_v}{W_p}\right) - 2R_p \left(\frac{W_v}{W_p}\right)\left(\frac{D_v - d_b}{2}\right) - \left(\frac{W_v}{W_p}\right)^2 \left(\frac{D_v - d_b}{2}\right)^2\right]$$

$$v_t = N_b K (W_p - W_v)$$

$$E_{cum} = \frac{\Delta E_b v_t t}{m_p}$$

where ΔE_b is the ball-impact energy (J/hit), v_t the ball-impact frequency (s^{-1}), ρ_b is the density of the balls, d_b the diameter of the balls, W_p the rotary speed of the supporting disk, W_v the rotary speed of the vial, *Dv* the diameter of the vial, *Rp* the distance between the rotational axes, N_b the number of balls, and *K* is a constant (which is approx. 1.5 for ball diameters around 10 mm), E_{cum} is the weight-normalized cumulative kinetic energy released in the system (J g^{-1}), *t* the milling time, and m_p the powder weight.

Phase transformation during milling was analyzed by powder X-ray diffraction. Fig. 1 shows the XRD patterns of the powders with the cumulated energy after milling. In Series A and B including C0, X-ray diffraction pattern shows the presence of the only initial powders: Mn_2O_3 (bixbyite, PDF 41-1442) and Fe_2O_3 (hematite, PDF 33-0664). Fe_2O_3 almost disappears in sample C5 and it is undetectable for C5, C10 and C20. In C20, the most intense lines of $MnFe_2O_4$ (PDF 38-0430) are observed.

The formation of a bixbyite structure $(Mn,Fe)_2O_3$, besides the presence of Fe_2O_3 and Mn_2O_3 precursor oxides, is unobservable. The only peaks that could be different from Mn_2O_3 bixbyite are $2\theta = 45.026°$ and 75.358° (λCr). In addition, the former has a value close to [2 0 2] diffraction line of $MnFe_2O_4$ (PDF 38-0430). If a solid solution of Fe into Mn_2O_3 structure occurs, this solid solution is undetectable from XRD analysis, due to the crystallite size reduction induced by the mechanical milling.

It is clear that the first mechanical grinding (series A and B) did not result in the formation of a new detectable phase, just led to the broadening of the diffraction peaks for the two types of initial oxides due to the reduction of the crystalline sizes and the accumulation of the lattice strains. However, a second observation can be made from the raw X-ray diffraction patterns. The intensity of the background scattering increases with milling time. This is called "temperature effect". The high energy ball milling together with the high local temperature, and the pressure generated may result in the displacement of atoms from their mean position leading to a partial breakdown of the conditions necessary for perfect destructive interferences between rays scattered at non-Bragg angles. This is called "temperature diffuse scattering"; it only contributes to the general background lines of the pattern [29].

Fig. 2 shows the average crystallite size values (*D*) versus the cumulated energy. These results show the variation of crystallite size and lattice strain in the samples. The average crystallite size (*D*) of the samples was estimated using the Scherrer equation. It can be seen that *D* variations are significant for both oxides. The crystallite size of grinded sample strongly diminished to around 20×10^5 J g^{-1} of the cumulative energy. The evolution was a linear diminution between approximately 0 and $\sim 20 \times 10^5$ J g^{-1} and then it was kept almost constant at around 2 nm. The crystal size of both pure oxides, Mn_2O_3 and Fe_2O_3, were in line with their respective specific surface area. Fig. 3 shows the relative intensity of the $2\theta = 49°$ XRD line, with respect to an internal standard (calcite). Those results show a behavior similar to that of the crystallite size, with some minor differences. Table 1 shows the cumulative energy and the specific surface area of each sample. Mn_2O_3 and Fe_2O_3 data are shown as reference. A0 and B0 showed a slow increase in the specific surface area with respect the weighted value of the pure oxides. Even taking into account the experimental error, this increase could indicate that 1 min of mechanical milling is sufficient to start the transformation of the solids. The A20 and B5 had a similar E_{cum}, 6.36 and 7.43×10^5 J g^{-1}, respectively. Their E_{imp} were in the same order and the relative XRD intensity was very close, but the time was 20 and 5 h, respectively. This fact reveals the importance of the cumulated energy instead of the time of milling. When B20 is compared to C5, the E_{imp} has a great difference (129 and 713 mJ, respectively). In both cases, the intensity of the XRD lines was similar, and it is

Table 1
Specific surface area of each sample, impact and cumulative energy of mechanical grinding and XPS atomic ratio.

Catalyst		Mean Mn oxidation state	S_{BET} fresh ($m^2\,g^{-1}$)	S_{BET} calc. ($m^2\,g^{-1}$)	Impact energy (mJ)	Frecuency of impact (vt, seg^{-1})	$E_{cumultive} \times 10^{-5}$ ($J\,g^{-1}$)	Mn/Fe atomic ratio XPS	O_{ad}/O_L ratio XPS
Mn_2O_3				28.7	–	–	–	–	–
Fe_2O_3				9.15	–	–	–	–	–
Serie A	A0	3.0	25.5	24	46	1152	0.01	3.0	0.3
	A5	3.0	27.2	26.2			1.59	–	–
	A10	3.0	29.7	25.2			3.18	–	–
	A20	3.1	27.3	23.5			6.36	–	–
Serie B	B0	3.0	25.8	25.8	129	1920	0.02	5.8	0.2
	B5	3.3	26.7	23			7.43	7.6	0.7
	B10	3.2	18.3	18.1			14.86	5.2	0.6
	B20	3.1	27.2	22.3			29.72	4.1	0.4
Serie C	C0	3.0	24.1	23.7	713	1181	0.09	–	–
	C5	3.1	11.6	9.3			25.26	–	–
	C10	2.9	14.7	8.9			50.52	–	–
	C20	2.8	13.2	5.7			101.05	1.7	0.2

possible that the crystal size diminished to a similar value. Thus, the impact energy does not contribute significantly to the textural transformations.

Due to the introduction of free energy in the crystal lattice during the milling process, when the raw materials are submitted to fracturing, deformation and welding, metastable phases are usually produced [30]. The main fraction of the excess enthalpy and modification of properties can mostly be assigned to the development of thermodynamically unstable states in the lattice, and not to the reduction of particle size. The active mechanical energy that is partially transferred is stored in the form of lattice defects [31]. The relaxations of these structural defects decrease the excess energy considerably, but never reach the initial state and consequently, a residual activity remains [32]. Initially, comminuting is the major process and in this case, only a small part of approximately 10 per cent of the excess enthalpy of the activated product may account for surface enlarging [33]. In Table 1, the specific surface area of each sample is shown. The value calculated on the basis of the specific surface area of the starting pure oxides is $\sim 24\,m^2\,g^{-1}$. At first, there is a weak increase in the specific surface area which may be exclusively attributed to the particle size diminution since no compound is capable of generating porosity. The catalysts do not change the textural properties. Only surface area changes are observed. Microporosity is not observed. The catalysts are mesoporous and the porosity is constant ($\sim 0.15\,cm^3\,g^{-1}$). The porosity of the precursors oxides remains the same and its mean values is $\sim$100 Å. The surface variations are only due to the changes in the particle size.

In the first step of the milling process, there is oxygen in the vial which may facilitate the increase of the manganese oxidation state from 3+ to 4+. It is well known that MnO_x with lattice defects shows a peak at low temperature in TPR experiments [33]. In Fig. 4a–d, TPR results are shown for all samples. The reduction profile of our Mn_2O_3 exhibits two well-defined peaks with the maxima at 374 and 477 °C in agreement with the TPR curves reported for bulk MnO_x catalysts [33]. Similarly, Fe_2O_3 exhibits two peaks: the first one well defined with a maximum at 375 °C, and an undefined peak at around 580 °C. The reduction sequence is probably MnO_2 or Mn_2O_3 to Mn_3O_4 and then, to MnO. The reduction of MnO to metallic manganese has not been observed even up to 950 °C because of its larger negative value of reduction potential [34,35]. During TPR experiment, it is expected that hydrogen easily reacts with Mn^{4+} or oxygen species coming from defective species of manganese oxide. This may be observed at the beginning of the TPR curve but with a very low intensity. The above mentioned peaks appeared between 200 and 300 °C and they were present in all samples in which the cumulated energy from mechanical milling was less than $10 \times 10^5\,J\,g^{-1}$. Samples A0 and B0 had the highest intensity. Then, the increase in the manganese oxidation number and/or the oxygen inclusion into the network of the manganese oxide is confirmed. Thus, the initial cumulated energy is mainly in the form of lattice defects which may include manganese in a high oxidation state. The presence of Mn^{4+} and/or defective species of manganese oxide modifies the following stage of reduction. In fact, the transition 3+ to 3+/2+ has a minor temperature of reduction compared to Mn_2O_3 oxide. The mobility of the lattice oxygen induced by the defective species could explain this behavior. Samples B10 and B20, with a cumulative energy higher than $10 \times 10^5\,J\,g^{-1}$, show an increase in T_{3+} to T_{3+} to T_{2+}. A similar observation could be extended to samples C5 and C10. This phenomenon indicates that some transformation in the solid system could occur. Those changes could be explained by the introduction of Fe^{3+} into the bixbiyte structure forming a solid solution. While Fe^{3+} and Mn^{3+} radii are 0.645 Å for both ions, the introduction of Fe^{3+} could reorder the bixbiyte structure leading to a diminution of the defects. This solid solution extended to the entire sample has been obtained with the same Mn/Fe atomic ratio by calcinations of the precursor by means of complexation with citric acid [10]. This is a stage in the solid state reaction between Mn and Fe to form the spinel phase, $MnFe_2O_4$, which should be accompanied by a modification in the Mn/Fe atomic ratio on the surface. In fact, the Mn/Fe atomic ratio obtained from XPS measurements increases until B5 and diminishes in the following samples. In addition, even though XRD was not the most adequate tool for this scale, after C5 XRD patterns of Fe_2O_3 disappeared and a part of iron was introduced into the bixbiyte to form a solid solution, after $10 \times 10^5\,J\,g^{-1}$ of cumulated energy. According to Duran et al. [10], iron introduction into the bixbiyte structure promotes a resistance to reduction of the manganese oxide which is observable from TPR results. In fact, the first peak of reduction (transition Mn^{3+} to Mn^{3+} and Mn^{2+}) increased their temperature value from B10; that is, the first step of mechanical milling included size diminution, increased of structural defects and coverage of iron oxide by manganese oxide. This migrated manganese oxide probably explains the first peak of reduction and may have a lower crystallinity to generate an amorphous structure.

The peaks of the precursors in the reaction mixture underwent a progressive broadening and lowering with milling time. This behavior is due to the continuous reduction of crystallite grain size, as a consequence of the repeated fracture of the powders induced by milling [36]. However, the higher diminution of the XRD patterns of iron oxide with respect to those of manganese oxide could be explained when the solid solution is started. Fe_2O_3 disappears and acquires the structure of the bixbiyte. Unlike thermal synthesis, in mechanical milling it is difficult to establish a clear limit for

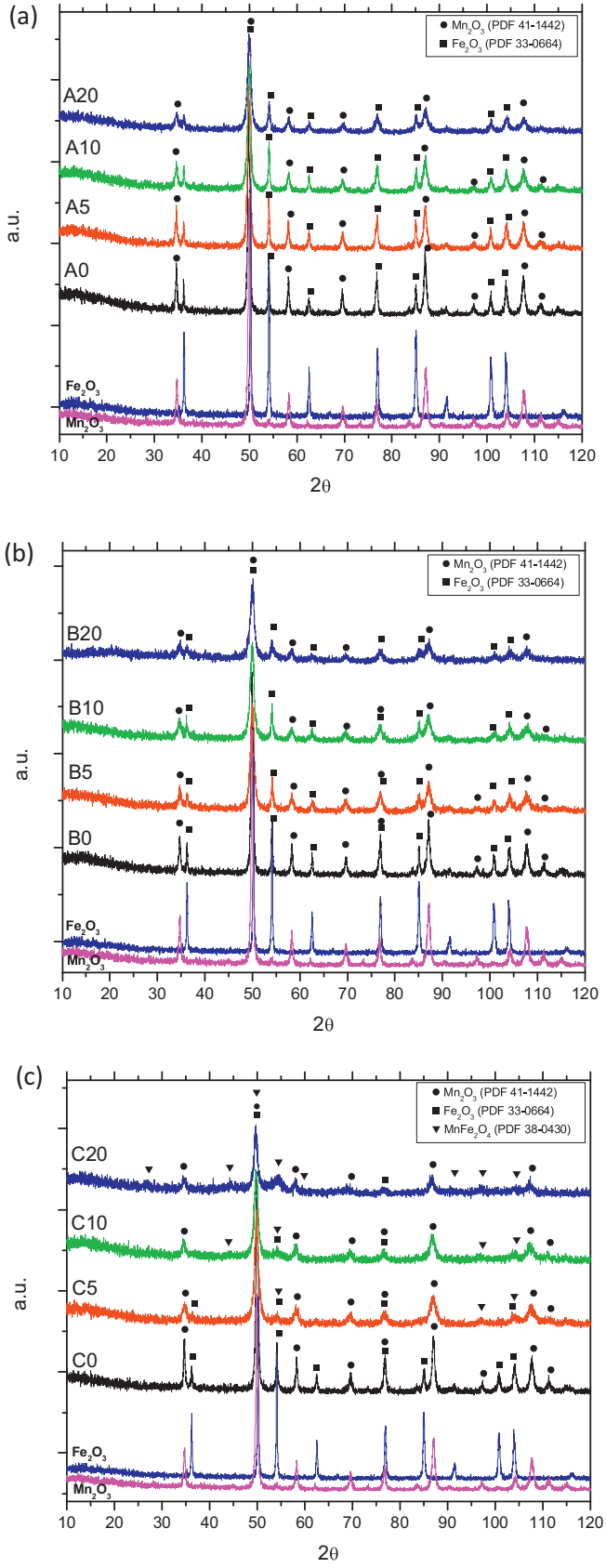

Fig. 1. XRD patterns of the samples with the cumulated energy after milling; (a) A series, (b) B series; (c) C series.

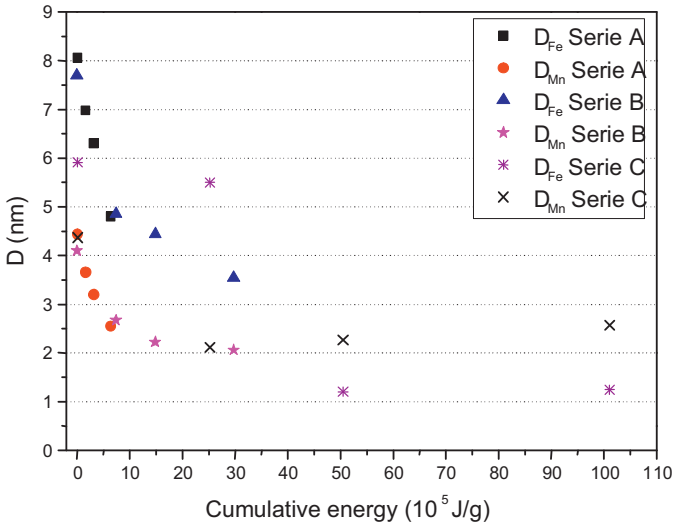

Fig. 2. *D*-values versus the cumulative energy.

each solid transformation and probably, a overlapping of each step takes place.

The following step of reaction included the partial reduction of manganese to form $MnFe_2O_4$. This spinel of manganese and iron has been extensively studied due to their magnetic properties. Mechanical milling studies have been performed with MnO or Mn_3O_4 as precursor to avoid the step of reduction, or with Mn_2O_3 and metallic Fe as precursors [39]. Those studies have been developed in Ar atmosphere. Scheme 1 shows the evolution of the solid system proposed.

In the vial, there is air and the initial oxidation presented in this work has been favored by the presence of oxygen. In fact, Medeiros et al. [19] working with Mn^{3+} and Fe^{3+} oxides as precursors and with a relatively low cumulated energy did not obtain the spinel structure. The XRD patterns of $MnFe_2O_4$ are clearly shown in C20, and are slightly hinted at C10 (PDF 38-0430 Iwakite). Although the surface is not representative of the bulk, the XPS results show a drastic decrease of the Mn/Fe ratio for C20, with a value of 1.7. This value is lower than the nominal one of the starting oxides. Mn/Fe atomic ration does no reach 0.5, due to the fact that Mn in excess is present under the MnO_x form. This XPS value could confirm the formation of the $MnFe_2O_4$ spinel. TPR results, Fig. 4c, clearly indicate a

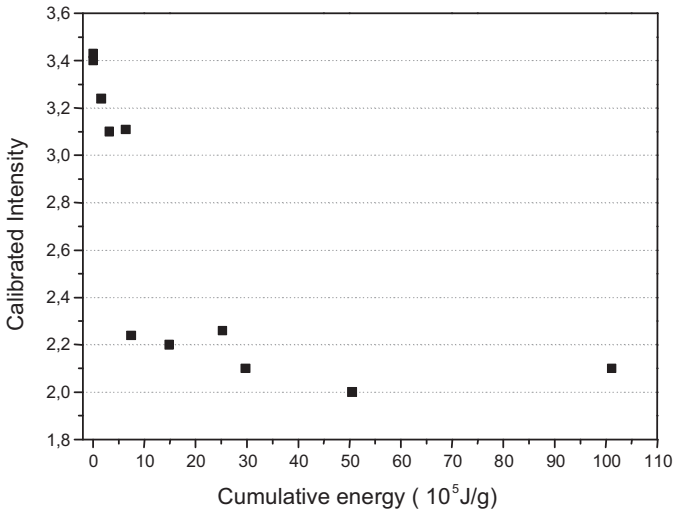

Fig. 3. XRD calibrated intensity versus cumulative energy.

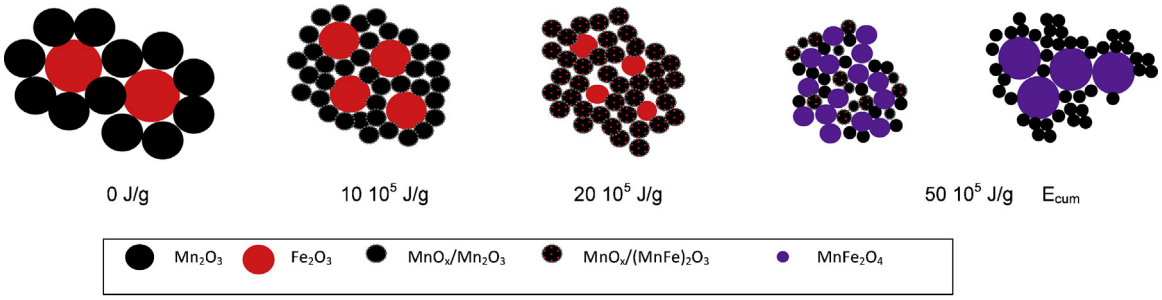

Scheme 1.

diminution of manganese species with an oxidation number higher than 2+ when the cumulated energy is increased. The average oxidation number is calculated from the hydrogen consumption, and those values are showed in Table 1. The spinel phase is deficient in iron because Mn^{3+} could replace it into the structure [36]. The appearance of the new phase implies a strong reduction of the specific surface area due to the disappearance of the small particles of Mn_2O_3 or $(Mn,Fe)_2O_3$, being both phases the main contribution to the specific surface area. In this respect, and following the specific surface area evolution above $20\,10^5\,J\,g^{-1}$ and an $E_{imp} = 713$ mJ, the system evolves to $MnFe_2O_4$. Although it is possible to obtain the spinel structure $MnFe_2O_4$ from Mn_2O_3 and Fe_2O_3 as precursors, it is necessary to control the atmosphere and provide a great amount of cumulated energy. Ding et al. [20] using stainless steel balls found that Mn_2O_3 and Fe_2O_3 ball-milled for 66 h under argon atmosphere resulted in the formation of disordered $MnFe_2O_4$. These authors also indicated that the Fe of the stainless steel ball could contaminate the sample and induce the formation of a wustite phase. Our results obtained after 20 h lead us to conclude that in order to get $MnFe_2O_4$, it is convenient to work at energy higher than that obtained with stainless steel balls.

Fig. 5 shows the catalytic performance of the catalyst per unit area of specific surface. The catalysts B5 and B10 have the best performance; this is better than the reference catalyst. C10 has also a good performance but their specific surface area is poor. However, this result indicates that some characteristics of the surface

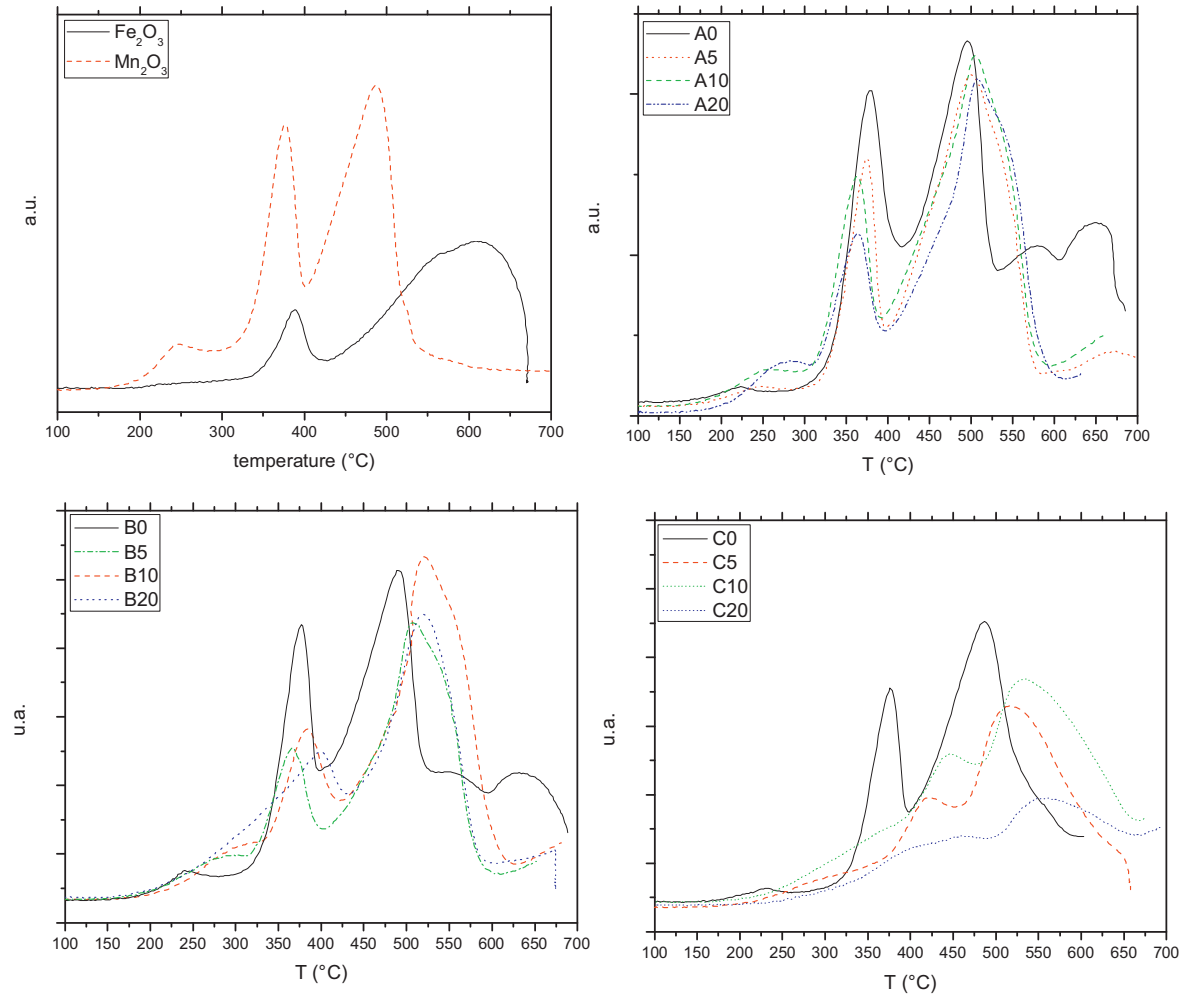

Fig. 4. TPR results.

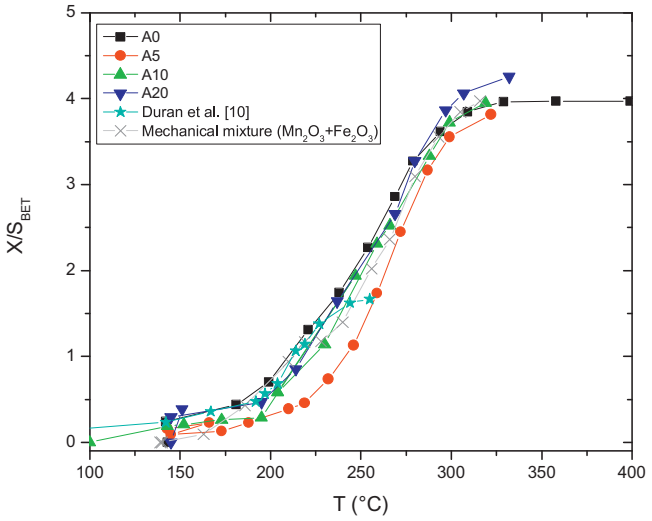

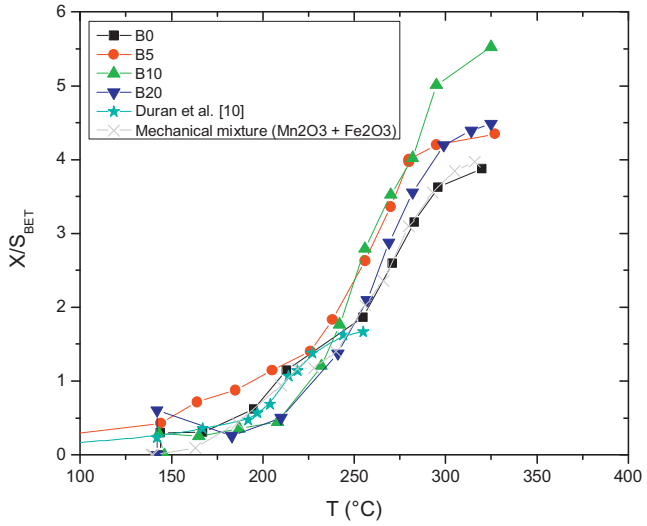

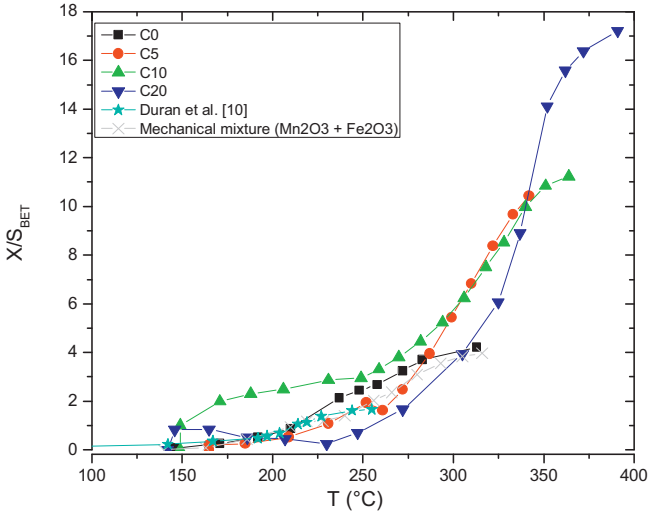

Fig. 5. Activity per unit area of specific surface versus temperature.

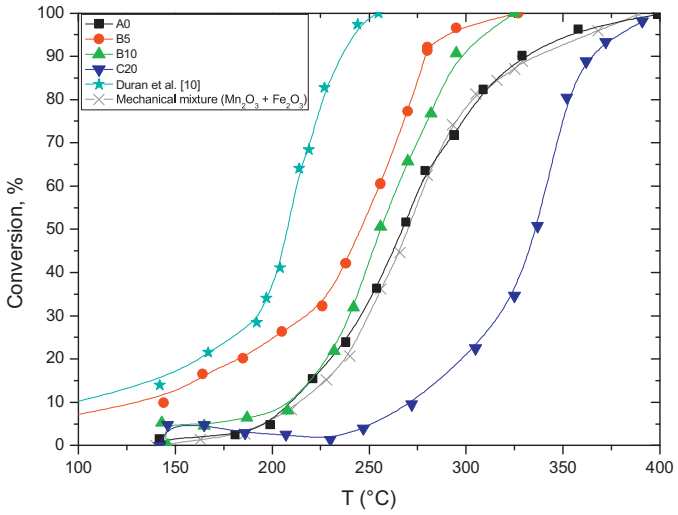

Fig. 6. Light-off curves in the *n*-hexane combustion for A0, B5, B10, C20, mechanical mixture (Mn:Fe 3:1) of $Mn_2O_3 + Fe_2O_3$, and Mn:Fe 3:1 synthesized by Duran et al. [10].

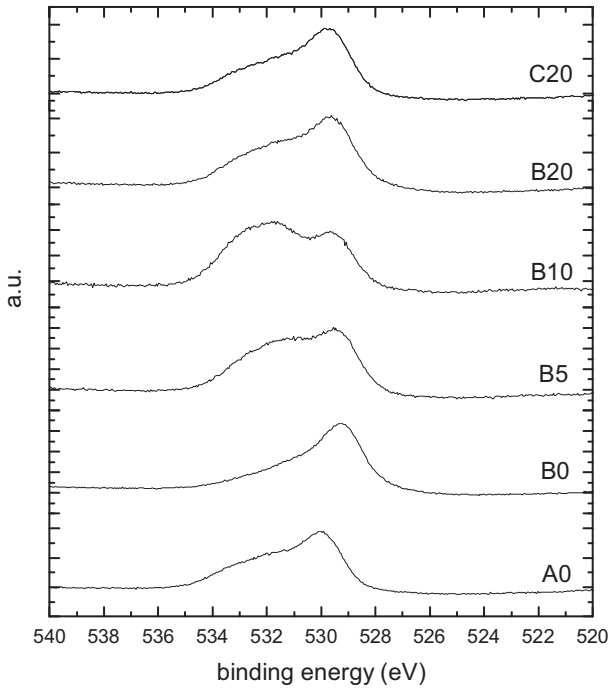

Fig. 7. O 1s peak obtained by XPS.

observed in B5 and B10 are present after $50 \times 10^5\,J\,g^{-1}$ of cumulative energy by milling. As an example of the catalytic importance of those results, Fig. 6 shows the light-off curves in the *n*-hexane combustion for A0, B5, B10, C20, mechanical mixture (Mn:Fe 3:1) of $Mn_2O_3 + Fe_2O_3$, and Mn:Fe 3:1 synthesized by Duran et al. [10]. Two possible mechanisms, a suprafacial and an intrafacial one and they are widely accepted now for oxidation reactions. The former mechanism arises from the interaction between surface oxygen and reactants and, for hydrocarbon oxidation, it is operative at low temperature ($T < 400\,^{\circ}C$). The latter involves a redox cycle, in which bulk oxygen migrates toward the surface becoming available for the oxidation of the substrate and it is replaced by gaseous oxygen through a Mars–van Krevelen mechanism. The actual mechanism of the catalytic reaction will be determined by the oxygen mobility in the crystalline framework as well as the catalyst affinity with

oxygen. It is proposed that paraffin oxidation would occur by means a suprafacial mechanism. The capacity for adsorbing oxygen of the catalyst is deduced from the O_{ad}/O_L ratio determined by XPS. O 1s decomposition was made following the conditions used by Merino et al. [40]. Fig. 7 shows the O 1s peak obtained by XPS.

The catalytic activity follows the O_{ad}/O_L ratio. In addition, it is well known that Mn^{4+} [33], defective species [37,38], and $(Mn,Fe)_2O_3$ solid solution [10] improve the catalytic performance of manganese oxides. On the contrary, Mn^{2+} is not a good catalyst for catalytic combustion. It is clear that, despite the diminution of the specific surface area, B5 characteristics improve the catalytic combustion properties as compared to the initial mechanical mixture. Besides the chemical composition, the catalyst obtained from mechanical milling exhibits unusual catalytic properties, due to their extremely small grain size or large specific surface area. Sample C20 shows a poor activity in *n*-hexane combustion due to the progress of the solid state reaction to $MnFe_2O_4$ and the specific surface area decrease.

4. Conclusions

The route of the solid state transformation of Mn–Fe–O system starting from manganese and iron oxides has been established as a function of the cumulated energy from mechanical milling. A description of the chemical and physical transformations has been done. From this study, it is possible to predict the milling conditions to obtain a Mn–Fe–O material with catalytic applications. That is, with an adequate specific surface area and an appropriate arrangement of phases.

The influence of the impact energy and the cumulated energy has been discriminated. In the same sense, the time factor and cumulated energy on the sample have been evaluated.

At high cumulative energy, it is possible to obtain the $MnFe_2O_4$ phase from Mn_2O_3 and Fe_2O_3 as precursors at relatively short times.

Complex multicomponent catalysts, which may be difficult to prepare by conventional high temperature treatment, could be successfully prepared by milling. Besides the chemical composition, the catalyst obtained from mechanical milling exhibits unusual catalytic properties, due to their extremely small grain size or large specific surface area.

Acknowledgments

The authors thank the financial support received from UNSL, CONICET and ANPCyT. They are also grateful to Dra. M. Roxana Morales for his assistance with XRD calibrated measurements. They are also grateful to ANPCyT for the purchase of the UHV Multi Analysis System (PME 8-2003).

References

[1] S.H. Tolbert, A.B. Herhold, L.E. Brus, A.P. Alivisatos, Phys. Rev. Lett. 76 (1996) 4384–4387.
[2] G.B. Gonzalez, T.O. Mason, J.P. Quintana, O. Warschkow, D.E. Ellis, J.H. Hwang, J.P. Hodges, J.D. Jrgensen, J. Appl. Phys. 96 (2004) 3912–3920.
[3] S.F. Mansour, M.A. Elkestawy, Ceram. Int. 37 (2011) 1175–1180.
[4] J. Mazo-Zuluaga, J. Restrepo, J. Mejia Lopez, Physica B 398 (2007) 187–190.
[5] Y. Komorida, M. Mito, H. Deguchi, S. Takagi, A. Millán, N.J.O. Silva, F. Palacio, Appl. Phys. Lett. 94 (2009) 202503.
[6] I. Fita, V. Markovich, D. Mogilyanski, R. Puzniak, A. Wisniewski, L. Titelman, L. Vradman, M. Herskowitz, V.N. Varyukhin, G. Gorodetsky, Phys. Rev. B: Condens. Matter 77 (2008) 224421.
[7] M. Suzuki, S.I. Fullen, I.S. Suzuki, Phys. Rev. B: Condens. Matter 79 (2009) 024118.
[8] B.P. Richards, A.C. Greenham, J. Appl. Phys. (J. Phys. D: Appl. Phys.) 2 (1) (1968) 1297–1302.
[9] C.C. Koch, Nanostruct. Mater. 9 (1–8) (1997) 13–22.
[10] F.G. Duran, B.P. Barbero, L.E. Cadus, C. Rojas, M.A. Centeno, J.A. Odriozola, Appl. Catal., B 92 (2009) 194–201.
[11] G.B. Schaffer, P.G. McCormick, Scr. Metall. 23 (6) (1989) 835–838.
[12] G.B. Schaffer, P.G. McCormick, Metall. Trans. A. 22 (1991) 3019–3024.
[13] P. Matteazzi, G. Le Caer, Mater. Sci. Eng., A. 149 (1991) 135–142.
[14] T. Kosmac, T.H. Courtney, J. Mater. Res. 7 (1992) 1519–1525.
[15] W.A. Kaczmarek, B.W. Ninham, IEEE Trans. Magn. 30 (1994) 732–734.
[16] S.J. Campbell, W.A. Kaczmarek, G.M. Wang, Nanostruct. Mater. 6 (1995) 735–738.
[17] S. Linderoth, J.Z. Jiang, S. Morup, Mater. Sci. Forum 235-238 (1997) 205–210.
[18] J.Z. Jiang, Y.X. Zhou, S. Morup, C.B. Koch, Nanostruct. Mater. 7 (1996) 401–410.
[19] S.N. de Medeiros, A. Luciano, L.F. Cotica, I.A. Santos, A. Paesano Jr., J.B.M. da Cunha, J. Magn. Magn. Mater. 281 (2004) 227–233.
[20] J. Ding, P.G. McCormick, R. Street, J. Magn. Magn. Mater. 171 (1997) 309–314.
[21] E.J. Bergey, L. Levy, X. Wang, L.J. Krebs, M. Lal, K. Kim, S. Pakatchi, C. Liebow, P.N. Prasad, Biomed. Microdevices 4 (2002) 293–299.
[22] M. Saferikova, L. Safarik, Magn. Electr. Separ. 10 (2001) 223.
[23] Y. Tamaura, Y. Ueda, J. Matsunami, N. Hasegawa, M. Nezuka, T. Sano, M. Tsuji, Sol. Energy 65 (1999) 55–57.
[24] Y. Tamaura, S. Steinfeld, P. Kuhn, K. Ehrensberger, Energy 20 (1995) 325–330.
[25] Y. Tamaura, M. Kojima, T. Sano, Y. Ueda, N. Hasegawa, M. Tsuji, Int. J. Hydrogen Energy 23 (1998) 1185–1191.
[26] H.H. Kedesdy, A. Tauber, J. Am. Ceram. Soc. 39 (1956) 425–431.
[27] N. Burgio, A. Iasonna, M. Magini, S. Martelli, F. Padella, II Nuovo Cimento D 13 (4) (1990) 459–476.
[28] T. Rojac, M. Kosec, B. Malic, J. Holc, J. Eur. Ceram. Soc. 26 (2006) 3711–3716.
[29] B.D. Cullity, Elements of X-ray Diffraction, second ed., Addison Wesley, Reading, MA, 1978.
[30] C. Suryanarayana, Prog. Mater. Sci. 46 (2001) 1–184.
[31] P. Pourghahramani, Ph.D. Thesis, Lulea University of Technology, 2006, ISSN 1402-1757.
[32] K. Meyer, Physikalisch-chemische Kristallographie, VEB Deutscher Verlag Fur Grundstoffindustrie, Leipzig, 1968, pp. 302–320.
[33] M.R. Morales, B.P. Barbero, L.E. Cadus, Appl. Catal., B 67 (2006) 229–236.
[34] J. Carno, M. Ferradon, E. Bjornborn, D. Jaras, Appl. Catal., A 155 (1997) 265–281.
[35] F. Kapteijn, L. Singredjo, A. Andreini, J.A. Moulijn, Appl. Catal., B 3 (1994) 173–189.
[36] C. Alvani, G. Ennas, A. La Barbera, G. Marongiu, F. Padella, F. Varsano, Int. J. Hydrogen Energy 30 (2005) 1407–1411.
[37] M.R. Morales, B.P. Barbero, L.E. Cadus, Fuel 87 (7) (2008) 1177–1186.
[38] F.N. Agüero, A. Scian, B.P. Barbero, L.E. Cadus, Catal. Lett. 128 (2009) 268–280.
[39] D. Chen, H.Y. Liu, L. Li, Mater. Chem. Phys. 134 (2012) 921–924.
[40] N.A. Merino, B.P. Barbero, P. Eloy, L.E. Cadus, Appl. Surf. Sci. 253 (2006) 1489–1493.